# Distributed Underwater Acoustic Source Localization and Tracking

Jun Ye Yu[1], Deniz Üstebay[1], Stephane Blouin[2], Michael Rabbat[1], and Mark Coates[1]
[1]Dept. of Electrical and Computer Eng., McGill University, Montréal, Québec, Canada
[2]DRDC, Atlantic Research Centre, 9 Grove Street, Dartmouth, Nova Scotia, Canada
Email: {jun.y.yu, deniz.ustebay}@mail.mcgill.ca, stephane.blouin@drdc-rddc.gc.ca,
{michael.rabbat, mark.coates}@mcgill.ca

*Abstract*—We consider the problem of localizing and tracking an acoustic noise source under water using bearing measurements taken from a small collection of acoustic sensors. Nodes must cooperate in order to improve their estimates and overcome significant noise levels and spurious measurements from clutter. However the underwater communication channel is highly unreliable, which makes coordination challenging. We evaluate the performance of distributed particle filtering methods in the setting where nodes communicate over unreliable links. Our results are validated using data from an experiment conducted at sea.

## I. INTRODUCTION

Networks of underwater acoustic sensors are designed for applications such as oceanographic data collection, seismic monitoring, offshore exploration, pollution monitoring, and marine mammal tracking [1], [2]. To facilitate deployment, such sensor nodes are usually battery-operated, which in turn requires energy-efficient and fault tolerant algorithms. Acoustic sensors inevitably face unpredictable and frequency-dependent attenuation, time-varying multipath effects, large Doppler and delay spreads, and limited bandwidth [3].

Common tasks for underwater sensor networks are the detection, localization, classification and tracking of an acoustic noise source of interest. In the present context, tracking refers to the sequential localization of a moving source from corrupted measurements. In a sensor network, these measurements are recorded by a set of sensor nodes. Given the unreliable and power-intensive nature of underwater acoustic communication, centralized processing of measurements is not viable. Instead, measurements must be processed by each node in the network and communications must be kept to a minimum. This way, the computational power of each sensor can also be exploited.

In this paper we study the performance of distributed tracking algorithms using data obtained in an underwater sensing experiment. In particular, we compare the performance of consensus-based distributed particle filtering algorithms. These methods require nodes to exchange distribution parameters. As an alternative, we also study exchanging measurements to run local particle filters at each node. In this case, we look at the effects of unreliable communication links as well. These results provide a realistic look at the tracking algorithms, which are generally assessed using synthetic data.

### A. Related Work

Tracking is a well-studied problem. When the system dynamics and measurements are linear with normally distributed noise components, the Kalman filter provides the optimal estimator. In this paper, we study data related to a source that turns sharply at times, making linear dynamics models unfit for the problem. A second nonlinearity arises from the measurements we have, bearing angle and range, which are nonlinear functions of the state. In this case, we resort to particle filters, which outperform the Kalman filter for non-linear and/or non-Gaussian problems [4].

Tracking in a distributed manner is attracting much attention with the recent advances in sensor technology and developments in distributed algorithms. There are mainly two approaches to distributed particle filters for wireless sensor networks (see [5] and references therein). The first approach relies on communicating the measurements to be processed at a leader node. Because of the unreliable nature of the underwater communication channel [3], relying on a single node to do all the processing and all other nodes to constantly communicate their measurements is not feasible, even when the node elected to be the leader changes over time. The second approach is based on reaching a consensus on particle weights or distribution parameters [6]–[8]. Such distributed filters rely on the assumption of conditional independence of the measurements made at each node given the source state. Because they are consensus-based, these methods result in having the desired estimate computed at each node.

### B. Paper Organization

Section II describes the experiment performed to collect the dataset and presents a detailed discussion of the dataset. Section III deals with the modeling of the source's dynamics as well as the measurements. In Section IV, we discuss the tracking algorithms and compare their performance on the dataset. Finally, Section V concludes with some remarks and a discussion of future work.

## II. EXPERIMENTAL SETUP

We study data from an at-sea experiment conducted in October 2012. This experiment took place in the Emerald Basin area of the Scotian Shelf [9] located southwest of Nova Scotia, Canada. The experiment followed a multistatic active sonar setup with five acoustic sensors, a single acoustic source,

and an echo-repeater in the water. The source emitted a 1-second linear-frequency modulated (LFM) sweep in the 1100-1500 Hz range every minute for approximately three hours. The echo-repeater acted as a secondary source by repeating the wavetrain emitted by the acoustic source. Therefore, each acoustic sensor received the direct energy from the source as well as the echoed energy from the echo-repeater. The acoustic sensors that are used in the experiment are functionally similar to commercial-off-the-shelf products such as the NAUTIC cube [10] and AMARS [11]. The source and echo-repeater were towed by different vessels and repeatedly described East-West tracks while the sensors drifted over time. The acoustic sensors, echo-repeater, and source were maintained at an approximate depth of 60 meters in waters that are 250 meters deep. Each one of them had a GPS attached providing their location.

In this paper, we concentrate on localization and tracking of the source and for this reason, we do not use the measurements related to the echo-repeater. Figure 1 depicts the trajectory of the source along with the trajectories of the sensors, which were freely drifting.
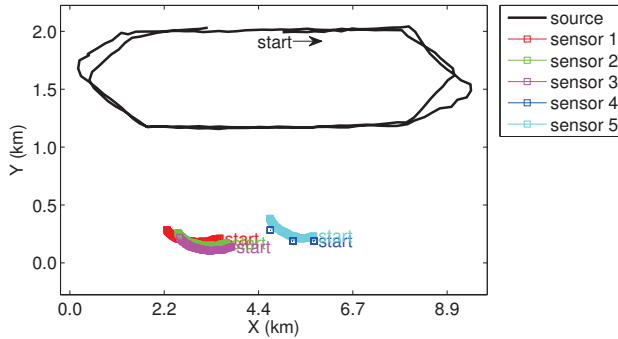


Fig. 1. Trajectories of the source and the sensors.

Underwater acoustic data were recorded on a central platform through radio data links. Fast-Fourier Transform and matched-filtering based on threshold detection [12] have been performed on the acoustic data, thus reducing each acoustic detection to a feature-triple comprised of a bearing angle (degrees), a time-of-arrival (seconds), and an SNR (dB).

The bearing is defined as the angle from the true North (the vertical axis of the Cartesian plane) to the line of sight between the observer and the source. The bearing angle is measured positive in the clockwise direction. Time-of-arrival (TOA) feature represents the time-of-flight of the acoustic wave in the water. We use the TOA information to compute the range according to

$$r = t_{\text{TOA}} \times \nu_{\text{sound}}, \qquad (1)$$

where $t_{\text{TOA}}$ is the time-of-arrival in seconds, $\nu_{\text{sound}} \approx 1.505$ km/s is the approximate speed of sound underwater, and $r$ is the range in kilometers. Figure 2 plots all three features of the measurements taken by Sensor 1; the measurements recorded by the other four sensors are similar but are not plotted here due to lack of space. The plots corresponding to the bearing and range also include the ground truth bearing and range values computed from the source and sensor locations.

Note that the measurements with less than 10dB of intensity are not included in the dataset. As demonstrated by Figure 2, the intensity (i.e., SNR) feature does not appear to provide any useful information and so this feature is not used in the methods considered in this paper.
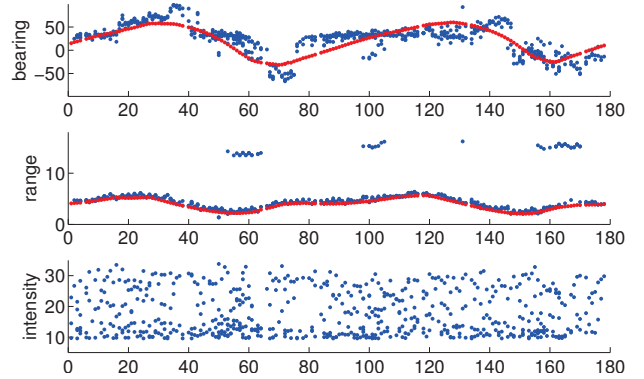


Fig. 2. Measurements from Sensor 1 (blue) and the ground truth (red) as a function of time (minutes). The units are: bearing in degrees, range in kilometers, intensity in dB.

Considering the entire set of measurements recorded by all five sensors, Figure 3 shows the bearing and range errors as a function of TOA. We observe that there is no correlation between TOA and bearing error. However, the range error is lower for low-TOA measurements. Also, as seen in Figure 2, the range information is mostly consistent with the ground truth except the measurements with very high TOA. This behavior can be explained by the confirmed temporary presence of another vessel during the experiment. Thus, we filter out the measurements with the range estimate greater than 9 kilometers (corresponding to TOA of more than 6 seconds). For the remaining measurements, we computed the correlation coefficient between the bearing errors and the range errors. The result is $-0.0448$, indicating no significant correlation between the two.
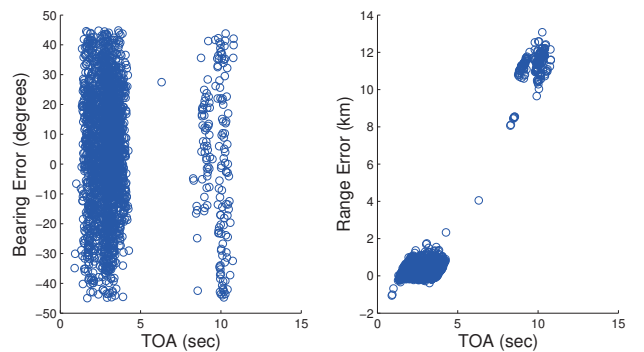


Fig. 3. Left: Bearing error (the difference between the measured bearing and the true bearing) vs. TOA. Right: Range error (the difference between the range computed from TOA and the true range) vs. TOA.

## III. THE DYNAMICS AND MEASUREMENT MODELS

We consider a state-space model of the problem. The state of the source at time $t$ is

$$\mathbf{x}_t = \begin{bmatrix} x_{t,1} & x_{t,2} & \dot{x}_{t,1} & \dot{x}_{t,2} \end{bmatrix}^T, \qquad (2)$$

where $x_{t,1}$ and $x_{t,2}$ correspond to the position in the $X$ and $Y$ coordinates in the Cartesian plane and $\dot{x}_{t,1}$ and $\dot{x}_{t,2}$ are the velocity values in these coordinates.

The dynamics of the maneuvering source are modeled using two different motion models [13]. We assume that at any time the source makes a motion $j \in \{1, 2\}$ out of the following two motions: (1) constant velocity (CV), or (2) clockwise coordinated turn (CT). The source moves according to one of these motion models with probabilities of $p_{CV}$ and $p_{CT}$, respectively, and $p_{CV} + p_{CT} = 1$. The state at time $t + 1$ is expressed as a function of the previous state $\mathbf{x}_t$ and process noise $\mathbf{v}_t$

$$\mathbf{x}_{t+1} = \mathbf{F}_t^j \mathbf{x}_t + \mathbf{G} \mathbf{v}_t, \tag{3}$$

where $\mathbf{F}_t^j$ is the transition matrix corresponding to the motion model $j \in \{1, 2\}$, and

$$\mathbf{G} = \begin{bmatrix} T^2/2 & 0 \\ 0 & T^2/2 \\ T & 0 \\ 0 & T \end{bmatrix}. \tag{4}$$

Here $T$ is the sampling interval and $\mathbf{v}_t \sim \mathcal{N}(0, \sigma_a^2 \mathbf{I}_{2\times 2})$ with scalar $\sigma_a$. The transition matrix corresponding to the constant velocity (CV) model is

$$\mathbf{F}_t^1 = \begin{bmatrix} 1 & 0 & T & 0 \\ 0 & 1 & 0 & T \\ 0 & 0 & 1 & 0 \\ 0 & 0 & 0 & 1 \end{bmatrix}, \tag{5}$$

whereas the coordinated turn (CT) model is governed by

$$\mathbf{F}_t^2 = \begin{bmatrix} 1 & 0 & \frac{\sin(\Omega_t T)}{\Omega_t} & -\frac{1-\cos(\Omega_t T)}{\Omega_t} \\ 0 & 1 & \frac{1-\cos(\Omega_t T)}{\Omega_t} & \frac{\sin(\Omega_t T)}{\Omega_t} \\ 0 & 0 & \cos(\Omega_t T) & -\sin(\Omega_t T) \\ 0 & 0 & \sin(\Omega_t T) & \cos(\Omega_t T) \end{bmatrix}. \tag{6}$$

The turning rate $\Omega_t$ is defined as

$$\Omega_t = \frac{a}{\sqrt{(\dot{x}_{t,1})^2 + (\dot{x}_{t,2})^2}}, \tag{7}$$

where $a > 0$ is the maneuver acceleration parameter. Note that the turning rate is a nonlinear function of the state.

The observing nodes form a graph $\mathcal{G} = (E, V)$ where $V = \{1, \ldots, n\}$ is the set of nodes, $n$ being the number of sensor nodes, and $E \subseteq V \times V$ is the set of bidirectional links such that $(u, v) \in E$ if nodes $u$ and $v$ can directly communicate. The location of the sensor node $v \in V$ is defined as $\mathbf{x}_t^v = \begin{bmatrix} x_{t,1}^v & x_{t,2}^v \end{bmatrix}^T$. We assume that each node is aware of its location.

The measurement of node $v$ at time $t$ is modeled as

$$\mathbf{z}_t^v = \mathbf{h}(\mathbf{x}_t, \mathbf{x}_t^v) + \mathbf{w}_t, \tag{8}$$

where $\mathbf{h}(\mathbf{x}_t, \mathbf{x}_t^v) = \begin{bmatrix} h_\theta(\mathbf{x}_t, \mathbf{x}_t^v) & h_r(\mathbf{x}_t, \mathbf{x}_t^v) \end{bmatrix}^T$. The measurement noise $\mathbf{w}_t$ has distribution

$$\mathbf{w}_t \sim \mathcal{N}(\begin{bmatrix} \mu_\theta \\ \mu_r \end{bmatrix}, \begin{bmatrix} \sigma_\theta^2 & 0 \\ 0 & \sigma_r^2 \end{bmatrix}). \tag{9}$$

The true bearing angle for node $v$ at time $t$ is

$$h_\theta(\mathbf{x}_t, \mathbf{x}_t^v) = \arctan\left(\frac{x_{t,1} - x_{t,1}^v}{x_{t,2} - x_{t,2}^v}\right), \tag{10}$$

whereas, the true range for the same node is

$$h_r(\mathbf{x}_t, \mathbf{x}_t^v) = \sqrt{(x_{t,1} - x_{t,1}^v)^2 + (x_{t,2} - x_{t,2}^v)^2}. \tag{11}$$

At each time step, a sensor node records zero or more measurements. We assume that each measurement is independent from others. The set of all measurements recorded by the sensors at time $t$ is denoted by $\mathbf{z}_t$.

## IV. TRACKING USING PARTICLE FILTERS

The goal is to obtain a state estimate for $\mathbf{x}_t$ using the measurements $\mathbf{z}_{1:t} = \{\mathbf{z}_1, \ldots, \mathbf{z}_t\}$ assuming that the dynamics model (3) and the measurement model (8) are known. Particle filters compute a posterior pdf $f(\mathbf{x}_t | \mathbf{z}_{1:t})$ from which an estimate for the state can be obtained (see [13] for an introduction to particle filters for tracking applications).

We present the results of simulations on the dataset described in Section II, using the models explained in Section III. The results are obtained from 1000 Monte Carlo trials. The parameters used are $T = 1$ minute, $p_{CV} = 0.85$, $a = 0.05$, $\sigma_a = 10^{-5}$, $\mu_\theta = 4°$, $\sigma_\theta = 25°$, $\mu_r = 0.4$km, and $\sigma_r = 1$km. The position components of the initial state $\mathbf{x}_0$ is modeled with a uniform distribution centered at the mean location of the five sensors. In particular, $x_{t,1} \sim \text{Uniform}(-2, 11)$, $x_{t,2} \sim \text{Uniform}(-2, 2)$ in kilometers. The velocity components are initialized with $\dot{x}_{t,1} \sim \text{Uniform}(-0.08, 0.24)$, $\dot{x}_{t,2} \sim \text{Uniform}(-0.11, 0.11)$ in kilometers/minute.

### A. Centralized particle filter

A centralized particle filter provides a performance benchmark for the scenarios discussed below. Here we implement a centralized bootstrap particle filter [14], assuming that sensor nodes send their measurements to a fusion center and all measurements are received by the fusion center. Figure 4 shows the performance of the centralized bootstrap filter as a function of the experiment time and also for a varying number of particles. The mean squared position error (MSE) at time $t$ is calculated as

$$\text{MSE}(t) = \frac{1}{K} \sum_{k=1}^{K} (x_{t,1} - \hat{x}_{t,1}^{(k)})^2 + (x_{t,2} - \hat{x}_{t,2}^{(k)})^2, \tag{12}$$

where $K = 1000$ is the number of Monte Carlo trials, $\hat{x}_{t,1}^{(k)}$ and $\hat{x}_{t,2}^{(k)}$ are the estimated position coordinates at time $t$ of the $k$th trial. Likewise, the time averaged squared position error (TASE) at the $k$th trial is calculated as

$$\text{TASE}(k) = \frac{1}{T} \sum_{t=1}^{T} (x_{t,1} - \hat{x}_{t,1}^{(k)})^2 + (x_{t,2} - \hat{x}_{t,2}^{(k)})^2, \tag{13}$$

where $T = 178$ minutes is the experiment duration.

### B. Local particle filters and tracking in unreliable networks

To eliminate the need for a fusion center, we first consider dissemination of measurements in the network. In this setting, each node runs a local particle filter using its own measurements and the measurements received from other sensors. We assume that the sensor nodes broadcast their measurements at every time step and that the graph topology is a complete
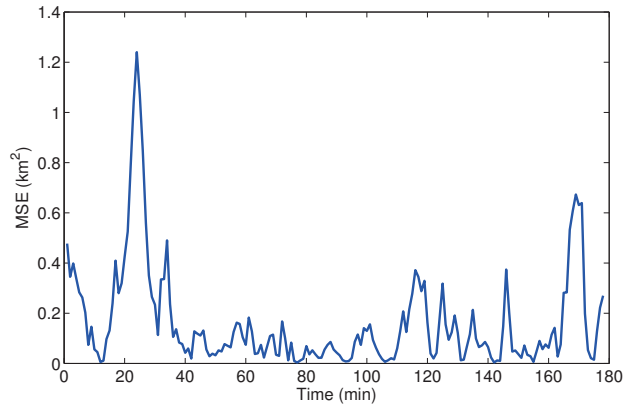
(a)
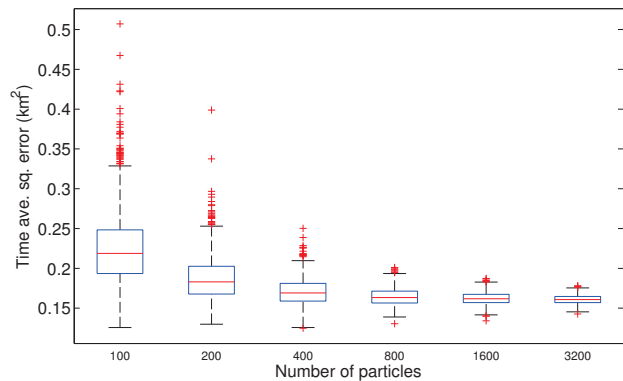


(b)

Fig. 4.    Performance of the centralized bootstrap particle filter. (a) Mean squared error over time for $N = 1600$ particles. (b) Time-averaged squared error vs. number of particles. The upper and lower limits of boxes correspond to the 25th and 75th percentiles and the red lines show the median over 1000 Monte Carlo trials. The vertical lines extend to approximately 99% of the data and the rest are assumed outliers, shown in red +.

graph, i.e., each node can communicate with every other node in the network. We also assume that the communication links are not perfect. Each measurement is received independently with probability $p$. Below we provide the results for varying this probability between $p = 0$ (i.e., no communication between nodes, each node uses only its own measurements) and $p = 1$ (i.e., all broadcasts being successfully received, each node runs a copy of the centralized particle filter).

Each node runs a 1600-particle filter. The tracks that have more than $1.5km^2$ error, which is the maximum error yielded by the centralized particle filter over 1000 trials, are considered as lost tracks. Figure 5 shows the squared error performance of the local particle filter at Sensor 2. Note that the $x$-axis starts at 0.3 instead of 0, because all the tracks are lost for $p < 0.3$. Figure 6(a) illustrates the change in the percentage of lost tracks for all nodes when $p$ is varied. For very low values of $p$, almost all tracks are lost, which emphasizes the need of communication for acceptable tracking performance. As $p$ increases, the tracking performance improves in terms of both the squared error and the percentage of lost tracks. Finally, Figure 6(b) plots the decrease in the disagreement for increasing $p$. The disagreement is defined as the squared error

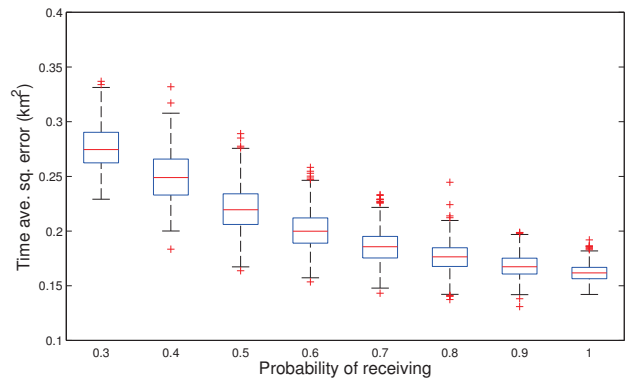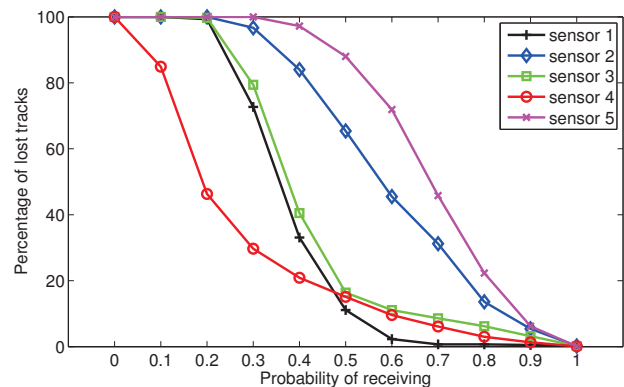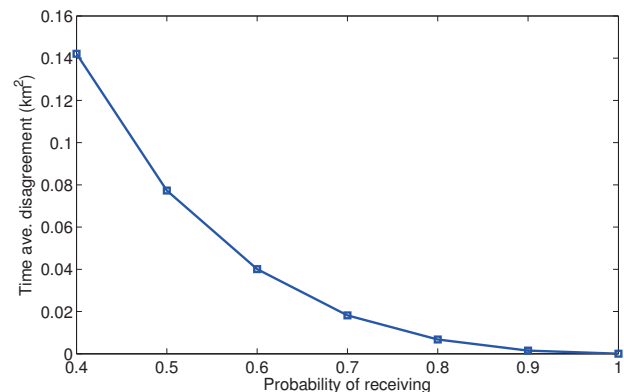between the average estimates of all pairs of nodes.



Fig. 5.    Time averaged squared error vs. $p$, the probability of receiving broadcasts for local filter at Sensor 2. The lost tracks are excluded.



(a)



(b)

Fig. 6.    Performance of the local bootstrap particle filters. (a) Percentage of lost tracks, which resulted more than $1.5km^2$ squared error, out of the total 1000 tracks. (b) Disagreement between sensors, averaged over time and pairs of nodes.

### C. Distributed particle filters

We implement a distributed version of the bootstrap particle filter, a Gaussian approximation particle filter [6], and the set membership particle filter [7]. Both the distributed bootstrap particle filter and the set membership particle filter assume that

the observations at different nodes are independent, and hence the global likelihood can be expressed as a multiplication of local likelihoods. The particle weights are then computed at each node via consensus. In addition to consensus on particle weights, the set membership particle filter also needs to run a session of maximum and minimum consensus for proposal adaptation. The Gaussian approximation algorithm, on the other hand, relies on the exchange of Gaussian parameters. In particular, each node approximates its local particle cloud with a normal distribution and the network reaches a consensus on a set of parameters that approximates the global posterior distribution with a Gaussian.

For all three filters, we assume that each transmission is a broadcast and the network has a complete graph topology. Therefore, to reach consensus, it is sufficient that each node broadcasts once assuming that no transmissions are lost.

Figure 7 depicts the performance of these three filters for varying number of particles. We observe that the Gaussian approximation particle filter has very poor performance whereas the other two methods perform similarly, and better than the Gaussian approximation filter in terms of percentage of lost tracks and mean time averaged squared error. It should be noted that set membership algorithm has significantly high computational complexity. Each node needs to process $5 \times N$ particles. The communication cost of the Gaussian approximation particle filter is on the order of $d + d^2$, where $d$ is the state dimension. The distributed bootstrap particle filter and the set membership particle filter need to compute the particle weights; hence, their communication cost is on the order of the number of particles.

## V. Conclusions

This paper presents results on distributed tracking of a maneuvering source using bearing and range measurements. In a more practical setting, it may not be possible to have access to the time-of-arrival values associated with the measurements and consequently to the range values. To accommodate such scenarios, we aim to extend our results to bearings-only tracking (i.e., without using range values). Another future work direction is the study of distributed algorithms in unreliable networks, as we have done above for local particle filters.

## References

[1] I. F. Akyildiz, D. Pompili, and T. Melodia, "Underwater acoustic sensor networks: Research challenges," *Ad Hoc Networks*, vol. 3, no. 3, pp. 257–279, 2005.

[2] J. Heidemann, W. Ye, J. Wills, A. Syed, and Y. Li, "Research challenges and applications for underwater sensor networking," in *IEEE Wireless Communications and Networking Conference*, vol. 1, 2006, pp. 228–235.

[3] M. Stojanovic and J. Preisig, "Underwater acoustic communication channels: Propagation models and statistical characterization," *IEEE Communications Magazine*, vol. 47, no. 1, pp. 84–89, 2009.

[4] A. Doucet, N. de Freitas, and N. Gordon, Eds., *Sequential Monte Carlo Methods in Practice*. New York: Springer-Verlag, 2001.

[5] O. Hlinka, F. Hlawatsch, and P. Djuric, "Distributed particle filtering in agent networks: A survey, classification, and comparison," *IEEE Signal Processing Magazine*, vol. 30, no. 1, pp. 61 –81, Jan. 2013.

[6] B. Oreshkin and M. Coates, "Asynchronous distributed particle filter via decentralized evaluation of Gaussian products," in *Proc. ISIF Int. Conf. Information Fusion*, Edinburgh,UK, July 2010.
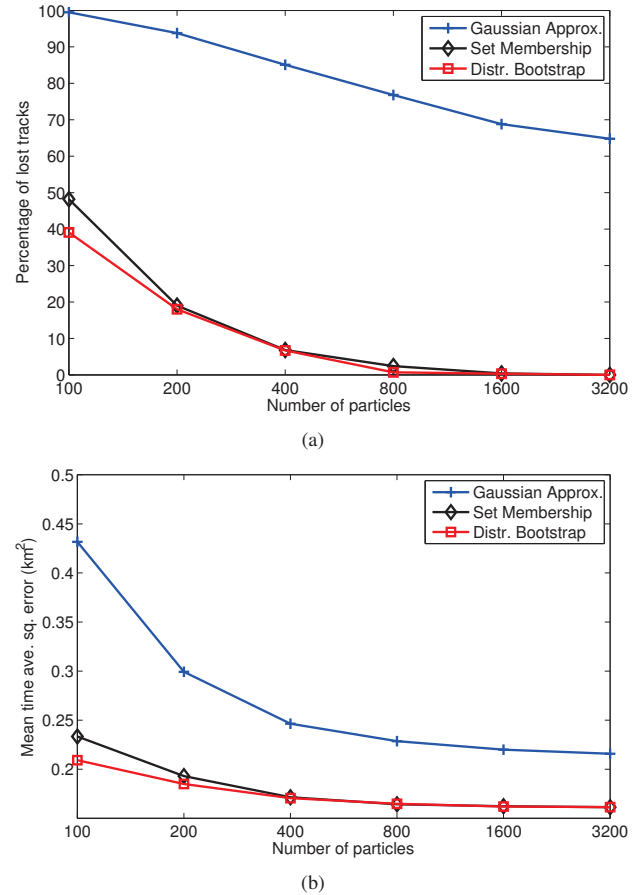
Fig. 7. Performance of distributed particle filters. (a) Percentage of lost tracks, which resulted more than $1.5km^2$ squared error, out of the total 1000 tracks, vs. number of particles. (b) Mean time-averaged squared error vs. number of particles.

[7] S. Farahmand, S. Roumeliotis, and G. Giannakis, "Set-membership constrained particle filter: Distributed adaptation for sensor networks," *IEEE Trans. on Signal Processing*, vol. 59, no. 9, pp. 4122–4138, Sept. 2011.

[8] D. Üstebay, M. J. Coates, and M. G. Rabbat, "Distributed auxiliary particle filters using selective gossip," in *Proc. IEEE Int. Conf. on Acoustics, Speech, and Signal Proc. (ICASSP)*, Prague, Czech Republic, May 2011, pp. 3296–3299.

[9] "The Scotian Shelf in context," in *State of the Scotian Shelf Report*. Department of Fisheries and Ocean, Canada.

[10] "Omnitech Electronics Inc." [Online]. Available: www.omnitechelectronics.ca

[11] "JASCO Research." [Online]. Available: www.jasco.com

[12] L. Qihu, *Digital Sonar Design in Underwater Acoustics: Principles and Applications*. Zhejiang University Press, Hangzhou and Springer-Verlag Berlin/Heidelberg, 2012.

[13] B. Ristic, S. Arulampalam, and N. Gordon, *Beyond the Kalman filter: Particle filters for tracking applications*. Artech House, 2004.

[14] N. Gordon, D. Salmond, and A. Smith, "Novel approach to nonlinear/non-Gaussian Bayesian state estimation," *IEE Proceedings-F*, vol. 140, no. 2, pp. 107–113, 1993.